In-Flight Alignment of Inertial Navigation System Using Line-Of-Sight Information

*Seung-Jin Oh[1],Dong-Bum Kim[2],Woo-Hyun Kim[3], Sang-Keun Jeong[4],
Hyung-Keun Lee[5], Jang-Gyu Lee[6]

[1/2/3/6]School of Electrical Engineering, Seoul Nat'l Univ.(E-mail: sky2943@snu.ac.kr
/dongbum1004@asrignc3.snu.ac.kr/ whyun77@snu.ac.kr / jgl@snu.ac.kr)
[4] Agency for Defense Development(E-mail: jfringe@add.re.kr)
[5] School of Electronics,Telecommunication&Computer Eng., Hankuk Aviation Univ.(E-mail:hyknlee@hau.ac.kr)

Abstract

This paper presents an in-flight alignment method for strapdown inertial navigation systems based on the line-of-sight information. Unlike the existing methods, the proposed method utilizes only the 2-axis angle measurements of the onboard image sensor and does not require any explicit range measurements between the vehicle and landmarks. To improve the accuracy of all the position, velocity, and attitude estimates through the in-flight alignment, an error model of the image-sensor-aided SDINS is derived. A simulation study demonstrates that the accuracy of SDINS can be improved by the line-of-sight information only.

Keywords: In-Flight Alignment, Image Sensor, Line-Of-Sight, Inertial Navigation System

1. Introduction

Benefits of combining a Global Positioning System (GPS) receiver and a StrapDown Inertial Navigation System (SDINS) are well known. In this hybrid scheme, the GPS receiver can provide position-type and velocity-type measurements to the SDINS at relatively low cost. As a result, the long-term accuracy can be ensured by the GPS measurements, and the short-term dynamic accuracy can be considered by the SDINS. In spite of the benefits of GPS/SDINS, practical difficulties arise in terms of the reliability, continuity, and availability due to vehicle dynamics, antenna direction, intentional jamming, and environmental interference. Thus, the SDINS errors need to be compensated by other aiding sensors[1][8].

To aid the SDINS with more reliability, continuity, and availability, this paper presents an efficient in-flight alignment method based on the line-of-sight (LOS) information. The most attractive feature of the proposed method is that it requires only the 2-axis LOS information to maintain or possibly to improve the accuracy of all the position, velocity, and attitude estimates. The utilized LOS information is measured by the pitch and yaw gimbal angles of the 2-axis image sensor. The LOS information is equivalent to the unit vector from the image sensor to the landmark whose position can be known in advance. Unlike the existing schemes, the proposed method requires no explicit range measurement between the vehicle and landmarks[3].

The in-flight alignment of the SDINS by the LOS information consists of two stages. At first, a known landmark in the captured image needs to be identified and tracked. Second, the LOS information is measured and utilized as the aiding measurement of the onboard Kalman filter. This paper mainly deals with the second topic, i.e., the utilization of the LOS information as the aiding measurement of the onboard Kalman filter. The first topic is beyond the scope of this paper but it is also an important research area for the future.

This paper is organized as follows. In the second section, the configuration of the two-axis image sensor is explained. The error model of the LOS-aided Kalman filter is presented. Finally, a simulation result demonstrates how much the LOS information can bound all the position, velocity, and attitude estimation errors.

2. Integration of Image Sensor and INS

Nowadays, it is not difficult to obtain a low-cost onboard image sensor, which provides the 2-axis line-of-sight (LOS) information. A commonly used configuration in image sensor systems is shown in Fig. 1.

As shown in Fig. 1, the outer gimbal can be rotated about the yaw axis. The inner pitch gimbal is suspended from the outer yaw gimbal. In Fig. 1, θ_s and ψ_s are the measurable gimbal angles [2]. The image sensor is placed on the pitch gimbal. A two-axes rate gyro is usually placed on the inner pitch gimbal measuring the angular velocities about the y- and z- axes. These rate measurements are utilized for the gimbals' stabilization.

When a 2-axis image sensor tracks a landmark's image at the center of the image plane, at least 4 frames are required to explain the related geometry. They are the navigation frame (n-frame), the body frame (b-frame), the image sensor frame (s-frame), and the landmark frame (l-frame) as summarized in Table 1. The configuration of the four frames is illustrated in Fig. 2.

The gimbal angles provided by an image sensor does not correspond to the angles between the b-frame and the n-frame, they indicate the relationship between the b-frame and s-frame.

The direction cosine matrix(DCM) C_s^n from the s-frame to the n-frame is decomposed into the DCM C_s^b from the s-frame to the b-frame and the DCM C_b^n from the b-frame to the n-frame.

$$C_s^n = C_b^n C_s^b \tag{1}$$

The Euler angles related with C_s^b and C_b^n summarized in Table 2.

For indirect feedback Kalman filter construction[4], Inertial Navigation System (INS) variables needs to be processed to form the same physical quantity provided by the external measurement. The difference between the INS-processed value and the measured value corresponds to the combination of the INS error states and the measurement error

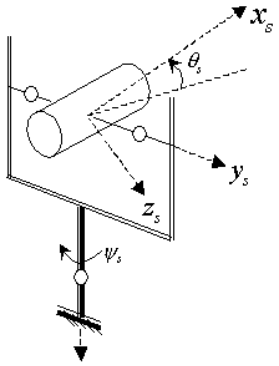

Figure 1. Image sensor configuration

Table 1. Definitions of coordinate systems.

Frame	Definition
i-frame	fixed coordinate with the center of the earth as the origin
n-frame	local level NED(North-East-Down) frame of which vertical axis is parallel with the gravity vector
b-frame	$x_b/y_b/z_b$: vehicle nose direction /right direction on the yaw plane /vertical downward direction ϕ_b, θ_b, ψ_b : vehicle roll, pitch, yaw attitudes
s-frame	$x_s/y_s/z_s$: image sensor heading / right direction on the yaw plane / vertical downward direction θ_s, ψ_s : image sensor pitch and yaw angle

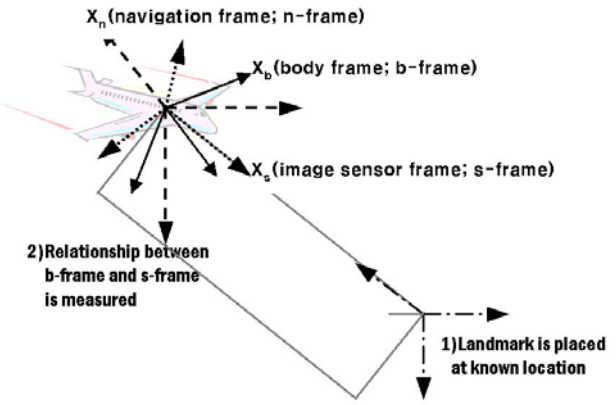

Figure 2. Configuration of related frames at landmark image acquisition

Table 2. Euler angle rotation between coordinate systems.

Transformation	Euler angle	Remarks
n-frame → b-frame	ψ_b, θ_b, ϕ_b	Measurement of Gyro
b-frame → s-frame	$\psi_s, \theta_s, 0$	Gimbal angles of image sensor

2.1 State space system model

For Kalman filter implementation, the system state vector $x(t)$ consists of the nine navigation error states and eight sensor bias error states.

$$\delta\dot{x}(t) = F(t)\ \ \delta x(t) + G(t)w(t) \quad , \quad w(t) \sim N(0,Q)$$
$$= \begin{bmatrix} F_{11} & F_{12} & 0_{3\times3} & 0_{3\times3} & 0_{3\times3} & 0_{3\times2} \\ F_{21} & F_{22} & F_{23} & F_{24} & 0_{3\times3} & 0_{3\times2} \\ F_{31} & F_{32} & F_{33} & 0_{3\times3} & F_{35} & 0_{3\times2} \\ 0_{3\times3} & 0_{3\times3} & 0_{3\times3} & 0_{3\times3} & 0_{3\times3} & 0_{3\times2} \\ 0_{3\times3} & 0_{3\times3} & 0_{3\times3} & 0_{3\times3} & 0_{3\times3} & 0_{3\times2} \\ 0_{2\times3} & 0_{2\times3} & 0_{2\times3} & 0_{2\times3} & 0_{2\times3} & 0_{2\times2} \end{bmatrix} \delta x(t) + \begin{bmatrix} 0_{3\times3} & 0_{3\times3} \\ C_b^n & 0_{3\times3} \\ 0_{3\times3} & -C_b^n \\ 0_{3\times3} & 0_{3\times3} \\ 0_{3\times3} & 0_{3\times3} \\ 0_{2\times3} & 0_{2\times3} \end{bmatrix} w(t) \tag{2}$$

where,

$$\delta x = [\delta L \quad \delta l \quad \delta h \mid \delta V_N \quad \delta V_E \quad \delta V_D \mid \delta\alpha \quad \delta\beta \quad \delta\gamma \mid \nabla_x \quad \nabla_y \quad \nabla_z \mid \varepsilon_x \quad \varepsilon_y \quad \varepsilon_z \mid \delta\theta_s \quad \delta\psi_s]^T$$

$[\delta\alpha \mid \delta\beta \mid \delta\gamma]^T$: attitude errors of inertial navigation system

$[\delta\theta_s \quad \delta\psi_s]^T$: bias errors of gimbal angle

$w(t)$: zero -mean white Gaussian process noise

Elements of the system matrix F in eq. (2) up to 15th order are the same as those in reference [5] and will be omitted for brevity.

2.2 Measurement model

We introduce a unit LOS vector as an indirect measurement. This indirect measurement will be applied to the Kalman filter. An indirect measurement model is explained from now on. As shown in Eq. (3), the measurement observation matrix H can be decomposed into the smaller matrices $H1$, $H3$, and $H6$ as shown in Eq. (3).

$$\begin{aligned} Z &= \widehat{e^n_{landmark}} - \widehat{e^n_{gimbal}} \\ &= H\,\delta x + v \\ &= [H1_{3\times3} \mid 0_{3\times3} \mid H3_{3\times3} \mid 0_{3\times3} \mid 0_{3\times3} \mid H6_{3\times2}]\delta x + v \end{aligned} \tag{3}$$

where,

$e^n_{landmark}$: unit vector derived from known position of landmark and vehicle's position

e^n_{gimbal} :unit vector derived from the image sensor's angle measurements and vehicle's attitude

$v \sim N(0,R)$: white-Gaussian measurement noise

☐ Derivation of $\widehat{e^n_{gimbal}}$

By Eq.(1), a unit vector of LOS $\hat{e}^n_{gimbal}$ can be derived from the attitude information of the vehicle and the gimbal angles of the image sensor. We assume that the LOS vector coincides with the x-axis vector of the image sensor frame. Thus, the LOS vector with respect to the n- frame is obtained as Eq.(4).

$$\hat{e}^n_{gimbal} = \hat{C}^n_s \begin{bmatrix} 1 & 0 & 0 \end{bmatrix}^T \tag{4}$$

The estimate $\hat{C}^n_s$ can be expressed as Eq.(5) with error terms.

$$\begin{aligned} \hat{C}^n_s &= C^n_s + \delta C^n_s \\ \hat{C}^n_s &= \hat{C}^n_b \tilde{C}^b_s = C^n_b (\mathrm{I} - \Phi) C^b_s (\mathrm{I} - \mathrm{E}) \end{aligned} \tag{5}$$

where

Φ : skew symmetric matrix made of the vehicle attitude error

E : skew symmetric matrix made of the gimbal angle error of the image sensor

The second-order term of the errors in Eq.(5) is small enough and thus can be ignored. As a result, δC^n_s is approximated as Eq.(6).

$$\begin{aligned} \delta C^n_s &= \hat{C}^n_s - C^n_s \\ &= -\hat{C}^n_s \mathrm{E} - \hat{C}^n_b \Phi \tilde{C}^b_s \end{aligned} \tag{6}$$

From Eqs. (4),(5), and (6), δe^n_{gimbal} can be expressed as follows.

$$\begin{aligned} \widehat{e^n_{gimbal}} &= e^n_{gimbal} + \delta e^n_{gimbal} \\ \delta e^n_{gimbal} &= \delta C^n_s \begin{bmatrix} 1 & 0 & 0 \end{bmatrix}^T \\ &= -\left[H3_{3\times 3} \mid H6_{3\times 2} \right] \left[\delta\alpha \quad \delta\beta \quad \delta\gamma \mid \phi_y \quad \phi_z \right]^T \end{aligned} \tag{7}$$

☐ Derivation of $\widehat{e^n_{landmark}}$

On the other hand, if the exact position of the landmark is known, the LOS vector can be computed differently from the previous method.

$$\widehat{e^n_{landmark}} = \widehat{D^n} \left(\left\| \widehat{D^n} \right\| \right)^{-1} \tag{8}$$

$$\widehat{D^n} = T^n_L \widehat{\Delta L} \tag{9}$$

$$\widehat{\Delta L} = \begin{bmatrix} L & l & h \end{bmatrix}^T_{landmark} - \begin{bmatrix} \hat{L} & \hat{l} & \hat{h} \end{bmatrix}^T_{INS} \tag{10}$$

$$T^n_L = \begin{bmatrix} R_m + h & 0 & 0 \\ 0 & (R_t + h)\cos L & 0 \\ 0 & 0 & -1 \end{bmatrix} \tag{11}$$

where, L : Latitude, l:longitude, h:hight

R_m: meridian radius of the earth

R_t: tangential radius of the earth

Eq. (10) denotes the latitude, longitude, and height increments of the vehicle from the landmark where the vehicle's position is estimated by INS. Eq.(11) denotes the transformation matrix from the latitude, longitude, and height values to the n-frame coordinate values.

Combining Eqs. (9) and (10), the following equations can be derived.

$$\widehat{D^n} = D^n + \delta D^n \tag{12}$$

$$\delta D^n = -T^n_L \begin{bmatrix} \delta L & \delta l & \delta h \end{bmatrix}^T_{INS} \tag{13}$$

$$\begin{bmatrix} \delta L & \delta l & \delta h \end{bmatrix}^T_{INS} = \begin{bmatrix} \hat{L} & \hat{l} & \hat{h} \end{bmatrix}^T_{INS} - \begin{bmatrix} L & l & h \end{bmatrix}^T_{vehicle} \tag{14}$$

By applying the perturbation method and the Taylor's series to Eq. (8), the estimated LOS vector $\hat{e}^n_{landmark}$ has the following error source.

$$H3 = \begin{bmatrix} \begin{bmatrix} [\cos\phi_b \sin\theta_b \cos\psi_b + \sin\phi_b \sin\psi_b] \\ [\cos\theta_s \sin\psi_s] \\ +[\sin\phi_b \sin\theta_b \cos\psi_b - \cos\phi_b \sin\psi_b][\sin\theta_s] \end{bmatrix} & \begin{bmatrix} [\cos\theta_b \cos\psi_b][\sin\theta_s] \\ +[\cos\phi_b \sin\theta_b \cos\psi_b \\ +\sin\phi_b \sin\psi_b][\cos\theta_s \cos\psi_s] \end{bmatrix} & \begin{bmatrix} [\sin\phi_b \sin\theta_b \cos\psi_b - \cos\phi_b \sin\psi_b] \\ [\cos\theta_s \cos\psi_s] \\ -[\cos\theta_b \cos\psi_b][\cos\theta_s \sin\psi_s] \end{bmatrix} \\ \begin{bmatrix} [\cos\phi_b \sin\theta_b \sin\psi_b - \sin\phi_b \cos\psi_b] \\ [\cos\theta_s \sin\psi_s] \\ +[\sin\phi_b \sin\theta_b \sin\psi_b + \cos\phi_b \cos\psi_b][\sin\theta_s] \end{bmatrix} & \begin{bmatrix} [\cos\theta_b \sin\psi_b][\sin\theta_s] \\ +[\cos\phi_b \sin\theta_b \sin\psi_b - \sin\phi_b \cos\psi_b] \\ [\cos\theta_s \cos\psi_s] \end{bmatrix} & \begin{bmatrix} [\sin\phi_b \sin\theta_b \sin\psi_b + \cos\phi_b \cos\psi_b] \\ [\cos\theta_s \cos\psi_s] \\ -[\cos\theta_b \sin\psi_b][\cos\theta_s \sin\psi_s] \end{bmatrix} \\ \begin{bmatrix} [\cos\phi_b \cos\theta_b][\cos\theta_s \sin\psi_s] \\ +[\sin\phi_b \cos\theta_b][\sin\theta_s] \end{bmatrix} & \begin{bmatrix} [\sin\theta_b][\sin\theta_s] \\ -[\cos\phi_b \cos\theta_b][\cos\theta_s \cos\psi_s] \end{bmatrix} & \begin{bmatrix} [\sin\phi_b \cos\theta_b][\cos\theta_s \cos\psi_s] \\ +[\sin\theta_b][\cos\theta_s \sin\psi_s] \end{bmatrix} \end{bmatrix}$$

$$H6 = \begin{bmatrix} -\begin{pmatrix} [\cos\theta_b \cos\psi_b][\sin\theta_s \cos\psi_s] \\ +[\sin\phi_b \sin\theta_b \cos\psi_b - \cos\phi_b \sin\psi_b][\sin\theta_s \sin\psi_s] \\ +[\cos\phi_b \sin\theta_b \cos\psi_b + \sin\phi_b \sin\psi_b][\cos\theta_s] \end{pmatrix} & \begin{pmatrix} [\cos\theta_b \cos\psi_b][-\sin\psi_s] \\ +[\sin\phi_b \sin\theta_b \cos\psi_b - \cos\phi_b \sin\psi_b] \\ [\cos\psi_s] \end{pmatrix} \\ -\begin{pmatrix} [\cos\theta_b \sin\psi_b][\sin\theta_s \cos\psi_s] \\ +[\sin\phi_b \sin\theta_b \sin\psi_b + \cos\phi_b \cos\psi_b][\sin\theta_s \sin\psi_s] \\ +[\cos\phi_b \sin\theta_b \sin\psi_b - \sin\phi_b \cos\psi_b][\cos\theta_s] \end{pmatrix} & \begin{pmatrix} [\cos\theta_b \sin\psi_b][-\sin\psi_s] \\ +[\sin\phi_b \sin\theta_b \sin\psi_b + \cos\phi_b \cos\psi_b] \\ [\cos\psi_s] \end{pmatrix} \\ -\begin{pmatrix} [-\sin\theta_b][\sin\theta_s \cos\psi_s] + [\sin\phi_b \cos\theta_b][\sin\theta_s \sin\psi_s] \\ +[\cos\phi_b \cos\theta_b][\cos\theta_s] \end{pmatrix} & \left([\sin\theta_b][\sin\psi_s] + [\sin\phi_b \cos\theta_b][\cos\psi_s] \right) \end{bmatrix}$$

$$\widehat{e^n_{landmark}} = e^n_{landmark} + \delta e^n_{landmark} \tag{15}$$

$$\widehat{e^n_{landmark}} = \frac{\widehat{D^n}}{\left\|\widehat{D^n}\right\|} = \frac{D^n}{\left\|D^n\right\|} + \frac{\partial}{\partial D^n}\left(\frac{\widehat{D^n}}{\left\|\widehat{D^n}\right\|}\right)\delta D^n + H.O.T. \tag{16}$$

Ignoring the high-order term in Eq. (16), $\delta e^n_{landmark}$ can be approximated as follows.

$$\begin{aligned}\delta e^n_{landmark} &= \frac{\partial}{\partial D^n}\left(\frac{\widehat{D^n}}{\left\|\widehat{D^n}\right\|}\right)\delta D^n \\ &= \left[H1_{3\times 3}\right]\left[\delta L \quad \delta l \quad \delta h\right]^T_{INS}\end{aligned} \tag{17}$$

3. Simulation results

A Monte-Carlo simulation was carried out to confirm the concept of the proposed alignment method. We assume that the vehicle makes an S-shaped trajectory to increase the observability by changing lateral acceleration and heading. The increased observability increases the estimability and the efficiency of the filter[6][7]. The important simulation parameters are summarized as follows.

- Total trial number of the simulation : 100
- Total Flight time of one trial : 240sec
- Velocity of the vehicle : 100m/s
- Number of landmark : 4(considering sensor's operating range)
- Measurement update : 1Hz
- Initial error
  - position(Lat,lon,hgt) : 40/R_0rad , 40/R_0rad, 10m
  - velocity(N,E,D) : 10m/s ,10m/s, 10m/s
  - attitude(roll,pitch,yaw) :1deg, 1deg,5deg

  * R_0: radius of the earth at the equator

The sensor specification values are summarized in Table 3.

In figure 3, it is shown that trajectory of image-sensor-aided INS(solid black line) follows the truth trajectory(dotted red line) well. This means the proposed system shows the stable performance in flight. This result means that the navigation error is compensated correctly by LOS information.

In Fig. 4, 5, and 6, the left plots show the error mean of position, velocity and attitude estimates, respectively. Each figure shows three times of fluctuations which occur at 60, 120, and 180 seconds. These fluctuations occur due to the transition of utilized landmarks during flight. This result shows that the landmark change causes the estimation error fluctuations.

Overall, it can be seen that the navigation errors bounded well which means that the designed Kalman filter works well. Figure 4 shows that the attitude error is within 0.5 degrees approximately and the. As shown in Fig. 5 and 6, the velocity and position errors are also bounded within 2m/s and 50m approximately.

The right plots of Fig. 4, 5, and 6 show comparison of one-sigma values computed by the Kalman filter error variance matrix and the error statistics of Monte-Carlo simulation. As time goes by, both one-sigma values approach to zero and show similar trend to each other. This means that the Kalman filter for the integration of the SDINS and the image sensor is designed well. Thus, it can be conclude that the in-flight alignment of SDINS is possible only by the 2-axis LOS information.

4. Conclusion

In this paper a new in-flight alignment method for the SDINS using LOS information from the image sensor is presented. A distinguishing feature of the proposed method is that only the 2-axis LOS information(gimbal angle) from an image sensor is sufficient for the SDINS in-flight alignment.

The error models to construct the image sensor/SDINS Kalman filter are explained. The performance of the proposed method is verified by a Monte-Carlo simulation. The simulation result shows that the in-flight alignment of SDINS is possible only by the 2-axis LOS information.

$$H1 = -\left[\begin{array}{c|c|c} \begin{pmatrix} D_{square}{}^{-\frac{1}{2}} - D_{square}{}^{-\frac{3}{2}}[R_m + h] \\ [L_{land} - \hat{L}_{ins}] \\ \left([R_m + h][L_{land} - \hat{L}_{ins}]\right)^T \end{pmatrix}(R_m + h) & \begin{pmatrix} -D_{square}{}^{-\frac{3}{2}}[R_m + h] \\ [L_{land} - \hat{L}_{ins}] \\ \left([(R_t + h)\cos L][l_{land} - \hat{l}_{ins}]\right)^T \end{pmatrix}((R_t + h)\cos L) & -\begin{pmatrix} -D_{square}{}^{-\frac{3}{2}}[R_m + h] \\ [L_{land} - \hat{L}_{ins}] \\ \left([-1][h_{land} - \hat{h}_{ins}]\right)^T \end{pmatrix} \\ \hline \begin{pmatrix} -D_{square}{}^{-\frac{3}{2}}[(R_t + h)\cos L] \\ [l_{land} - \hat{l}_{ins}] \\ \left([R_m + h][L_{land} - \hat{L}_{ins}]\right)^T \end{pmatrix}(R_m + h) & \begin{pmatrix} D_{square}{}^{-\frac{1}{2}} - D_{square}{}^{-\frac{3}{2}} \\ [(R_t + h)\cos L][l_{land} - \hat{l}_{ins}] \\ \left([(R_t + h)\cos L][l_{land} - \hat{l}_{ins}]\right)^T \end{pmatrix}((R_t + h)\cos L) & -\begin{pmatrix} -D_{square}{}^{-\frac{3}{2}}[(R_t + h)\cos L] \\ [l_{land} - \hat{l}_{ins}] \\ \left([-1][h_{land} - \hat{h}_{ins}]\right)^T \end{pmatrix} \\ \hline \begin{pmatrix} -D_{square}{}^{-\frac{3}{2}} \\ [-1][h_{land} - \hat{h}_{ins}] \\ \left([R_m + h][L_{land} - \hat{L}_{ins}]\right)^T \end{pmatrix}(R_m + h) & \begin{pmatrix} -D_{square}{}^{-\frac{3}{2}}[-1][h_{land} - \hat{h}_{ins}] \\ \left([(R_t + h)\cos L][l_{land} - \hat{l}_{ins}]\right)^T \end{pmatrix}((R_t + h)\cos L) & -\begin{pmatrix} D_{square}{}^{-\frac{1}{2}} - D_{square}{}^{-\frac{3}{2}}[-1] \\ [h_{land} - \hat{h}_{ins}] \\ \left([-1][h_{land} - \hat{h}_{ins}]\right)^T \end{pmatrix} \end{array}\right]$$

$$where,\ D_{square} = \left([R_m + h][L_{land} - \hat{L}_{ins}]\right)^2 + \left([(R_t + h)\cos L][l_{land} - \hat{l}_{ins}]\right)^2 + \left([-1][h_{land} - \hat{h}_{ins}]\right)^2$$

Acknowledgement

This work has been supported by Automation and Systems Research Institute (ASRI) in Seoul National University and Agency of Defense Development(ADD).

Table 3. Sensor error specification values

Error		std	unit
Accelero -meter	Scale factor	200	ppm
	Nonorthogonality	10	arcsec
	White noise	5	μg
	Random constant	100	μg
Gyro	Scale factor	20	ppm
	Nonorthogonality	10	arcsec
	White noise	0.01	deg/hr
	Random constant	0.01	deg/hr
Image sensor	Scale factor	0.04	deg
	White noise	0.17	deg

The results about IFA process are shown in the following Figures.

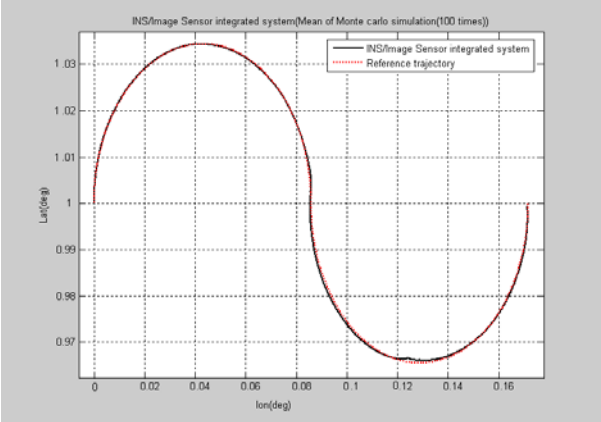

Figure 3. Simulation trajectory

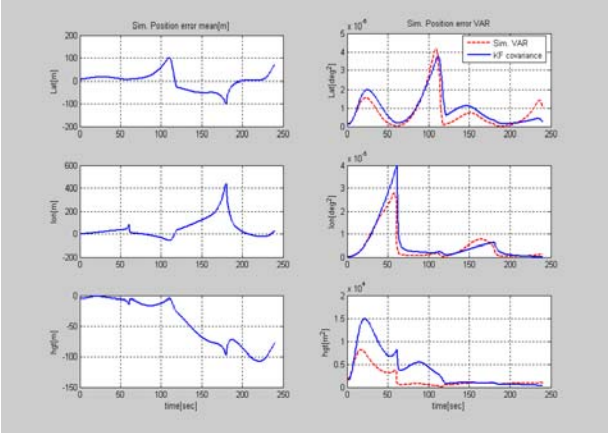

Figure 4. Trend of attitude error

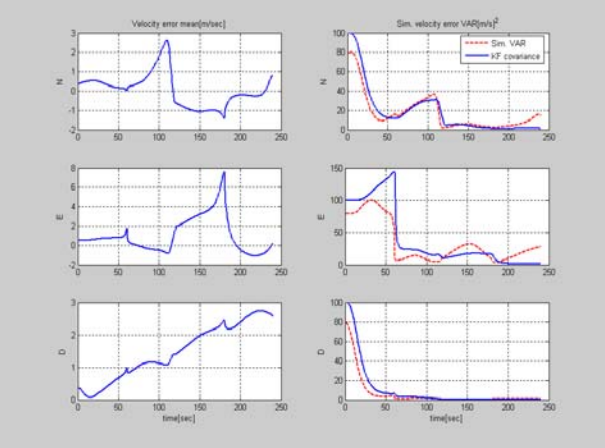

Figure 5. Trend of velocity error

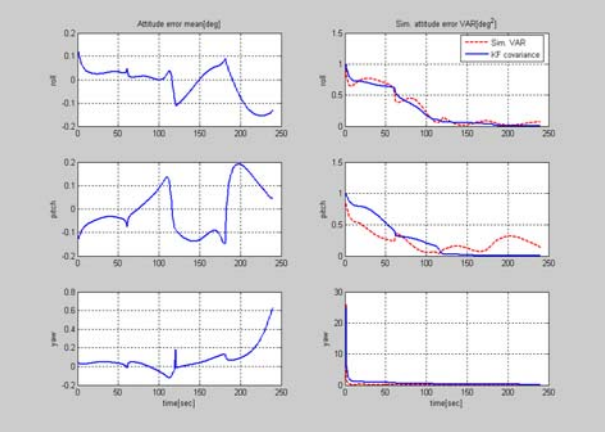

Figure 6. Trend of position error

Reference

1. D.H.Titterton, J.L.Weston, *Strapdown inertial navigation technology*, Peter Peregrinus Ltd., pp. 363~382, 1997
2. Ekstrand, B., "Tracking Filters and Models for Seeker Applications", *IEEE Trans. On Aerospace and Electronic Systems*, vol. 37, pp. 965-977, 2001.
3. George M.Siouris, *Missile Guidance and Control Systems*,Springer, pp.102~103, 2004
4. P.S. Maybeck(1994), *Stochastic Models, Estimation, and Control*, Vol.1, Navtech Book & Software Store pp.291~297.
5. Young Bum Park(2001), "Design of Integrated INS/GPS/-Odometer Navigation System and Its Performance Analysis," *School of Electronical Engineering and Computer Science, Seoul National University.*
6. D.Goshen-Meskin, I.Y. Bar-Itzhack, "Observability Analysis of Piece-Wise Constant Systems, *IEEE*, Vol.28, No.4, pp.1056~1075 (1992)
7. Goshen-Meskin, D., and Bar-Itzhack, I. Y. (1992)Observability analysis of piece-wise constant systems—Part II: Application to inertial navigationin-flight alignment. *IEEE Transactions on Aerospace and Electronic Systems*, 28, 4 (1992), 1068–1075
8. Joon Goo Park, Jin Won Kim, Jang Gyu Lee, Chan Gook Park, Gyu In Jee, Jong Taek Oh, "The Enhancement of INS Alignment Using GPS Measurements," *IEEE Position Location and Navigation Symposium* '98, Palm Springs, California, USA, April 20-23, 1998. pp.534-540.